Single Point Positioning with Vertical Total Electron Content estimation based on single epoch data

Artur Fischer[1], Sławomir Cellmer[1], and Krzysztof Nowel[1]

[1]Department of Geodesy, University of Warmia and Mazury, Olsztyn, 10-719, Poland

Correspondence to: Artur Fischer (artur.fischer21@gmail.com)

Abstract. This paper proposes a new mathematical method of ionospheric delay estimation in single point positioning (SPP) using a single-frequency receiver. The proposed approach focuses on the *ΔVTEC* component estimation (MSPPwithdVTEC) with the assumption of an initial and constant value equal to 5 in any observed epoch. The principal purpose of the study is to examine the reliability of this approach to become independent from the external data in the ionospheric correction calculation process. To verify the **MSPPwithdVTEC**, the SPP with the Klobuchar algorithm was employed as a reference model, utilizing the coefficients from the navigation message. Moreover, to specify the level of precision of the **MSPPwithdVTEC**, the SPP with the IGS TEC map was adopted for comparison as the high-quality product in the ionospheric delay determination. To perform the computational tests, real code data was involved from three different localizations in Scandinavia using two parallel days. The criterion were the ionospheric changes depending on geodetic latitude. Referring to the Klobuchar model, the **MSPPwithdVTEC** obtained a significant improvement of 15 – 25% in the final SPP solutions. For the SPP approach employing the IGS TEC map and for the **MSPPwithdVTEC**, the difference in error reduction was not significant, and it did not exceed 1.0% for the IGS TEC map. Therefore, the **MSPPwithdVTEC** can be assessed as an accurate SPP method based on error reduction value, close to the SPP approach with the IGS TEC map. The main advantage of the proposed approach is that it does not need external data.

1 Introduction

Single point positioning (SPP) allows of the indication of an autonomous position of a receiver using code data from the Global Positioning System (GPS). Code ranges are not ambiguous and do not require to apply the precise method of ambiguity initialization (Bakuła, 2020). The principal problem of SPP stems from different types of errors degrading the GPS signal between a rover and a specified satellite in a given epoch. Ionospheric delay contributes to the general GPS error budget by its volatility in the range of 40 – 60 m during daytime and 6 – 12 m at night (US Army Corps of Engineers, 2003).

The ionosphere consists of charged particles that appear because of the ionization process (El-Rabbany, 2002; Awange, 2012). Problems with ionosphere modeling come from difficulties between solar activity and the geomagnetic field interactions (Xu and Xu, 2016). The basic concepts of the GPS signals delay were briefly considered by Golubkov et al. and Kuverova et al. (Golubkov et al., 2018; Kuverova et al., 2018; Golubkov et al., 2019). To specify a suitable magnitude of

30   delayed GPS signal along an appropriate path between satellite and receiver, a proportional quantity such as Total Electron

31   Content (TEC) has to be involved and defined as the linear integral of the density of the particles alongside the ray path

32   (Cooper et al., 2019). The TEC unit is equal to 10^{16} electrons per square meter (in the cross-section of 1 m^2) (Ciraolo, 2005).

33   To calculate and reduce such effect on the GPS code measurement, Stępniak (2016) distinguished different types of models

34   and mathematical estimating methods: physical - theoretical (e.g. Chapman's model), physical - empirical (e.g. IRI and the

35   NeQuick model), mathematical - deterministic (based on a mathematics function), and mathematical – stochastic (based on a

36   large set of processed data used to describe the spatial-temporal changes of ionosphere) e.g. the IGS model.

37   The authors propose the autonomous SPP approach with $\Delta VTEC$ component estimation using single-frequency GPS

38   code observations to be independent of external products, e.g. an IGS TEC map. The disadvantage of the mathematical

39   models is performing an ionospheric effect calculation mostly in post-processing. Since many mathematical approaches to

40   self-sufficient ionospheric delay modeling have been proposed, especially in the carrier phase domain using multi-frequency

41   observations, the authors wanted to introduce a new estimation method employing single-frequency GPS code observations.

42   For instance, Georgiadiou (1994) proposed a mathematical method based on differences between the pseudo-ranges

43   measured on the L1 and L2 carries frequency, respectively (dual-frequency method). The computational tests with

44   comparison to the reference method without ionospheric corrections were done by Camargo et al. (2000), focusing

45   particularly on the pseudo-ranges filtered by the carrier phase. The method of slant delay estimation (STEC – alongside a

46   line of sight) in the L1 carrier reduced 80% of errors related to ionospheric effects in the point positioning technique, also

47   delivering improvement solutions during the ionosphere maximum. Bosy (2005) described a geometry-free linear

48   combination which can be employed to ionosphere modeling, with simultaneous consideration and repair of cycle-slip

49   effects and other parameters of GPS vector - ambiguity and tropospheric effects. Krypiak-Gregorczyk and Wielgosz (2018)

50   proposed the use of multi-frequency GNSS signals for TEC modeling, utilizing the carrier phase bias of a geometry-free

51   linear combination. The received bias accuracy results on the level of 7 – 8 cm allow TEC computation with desirable

52   uncertainty, i.e. lower than 1 TECU. Additionally, an ionosphere-free linear combination as an independent positioning

53   approach can also be well adapted to minimize the ionosphere negative impact on GPS positioning (Teunissen and

54   Kleusberg, 1998). However, Hofmann-Wellenhof et al. (2008) stated that "ionosphere-free" is not an entirely correct name,

55   caused by the approximation existing in the process of making the refractive index. Those authors studied an ionosphere-free

56   approach in the code SPP and achieved a beneficial magnitude of error reduction (50-60%) in relation to the reference SPP

57   model without ionospheric corrections.

58   On the contrary, empirical models do not significantly reduce the ionosphere influence in the GPS positioning as

59   mathematical (deterministic) methods, but can make real-time improvements by using the external data, e.g. coefficients

60   transmitted in the navigation message to correct the signal pseudo-ranges. One of these is the Klobuchar algorithm (see

61   Klobuchar, 1987), which compensates for 50 – 60% of the ionospheric range error, utilizing a single-layer model of the

62   ionosphere (Leick et al., 2015). In the current study, the authors wanted to treat the SPP method with the Klobuchar

63   algorithm as a reference method, because of its popularity and utility in GPS measurement. A significant improvement can

64 be noted in the vertical component which is the most affected by the atmospheric delay. Júnior et al. (2019) investigated the

65 analysis of the Klobuchar model in the ionospheric delay reduction procedure utilizing code observation in point positioning.

66 The algorithm works clearly when ionosphere activity is significant and improves vertical solutions by 67%. For the

67 horizontal components, the improvement using the Klobuchar algorithm is up to 9% regarding the non-iono model. It should

68 be noted that GPS point positioning using the Klobuchar algorithm can degrade the position because of the constant value of

69 the ionospheric delay (up to 5 ns SET) during nighttime.

70   High-quality representation of the ionosphere influence on positioning can be obtained by the Global Ionospheric

71 Models (GIMs), used mostly in the post-processing purposes as explained in Ciećko and Grunwald (2020). It is worth noting

72 that Abdelazeem et al. (2016) developed the regional ionospheric model over the European area and implemented it in

73 Precise Point Positioning (PPP), operating in real-time using the real-time service products (RTS) of the International GNSS

74 Service (IGS). The results present an improvement in the accuracy on the level of 40 % (under the mid-latitude region) in the

75 3D position relating to the IGS-GIM. The accuracy is higher primarily because of the better temporal and spatial resolution

76 of the model (15' and 1° x 1°), while the IGS TEC map includes nodes containing the appropriate VTEC value with a time

77 resolution of 1 hour and a spatial resolution of 2.5° x 5°, respectively for latitude and longitude. In turn, Krypiak-Gregorczyk

78 et al. (2017) prepared the ionosphere model covering the Europe region as well, based on multi-GNSS data. The solutions

79 are beneficial because they have 2-3 times lower RMS value than the results of GIMs, e.g. from IGS. Zhang et al. (2019)

80 also examined global ionospheric maps operating in real-time, dedicated to single-frequency positioning. Chen and Gao

81 (2005) tested the IGS TEC map as the basic condition to assess the precision of the PPP model using different procedures to

82 resolve the ionospheric delay problem such as single-frequency ionosphere-free linear combination (averages un-differenced

83 code and carrier-phase observations on the same frequency) or estimation of the ionospheric effect as an unknown

84 parameter. The advantage of the methods is no need for external products. For instance, the estimation method achieved

85 comparable accuracy in the mid-latitude stations but for the higher latitude, the GIM is still quite better, inversely on the

86 equatorial stations. This encourages a focus on the IGS TEC map as the high accuracy product to authenticate solutions from

87 the suggested approach to SPP, and to validate the autonomous method of the ionospheric delay calculation. It should be

88 noted that although the efficiency of GIMs is not significant using GPS code observations, the accuracy is suitable enough

89 for navigation goals and further development of this concept.

90   In sum, the motivation of this paper is to analyze a new mathematical method of ionospheric delay estimation to

91 improve the SPP. The authors put forward the hypothesis to be independent of external data use in the meaning of the new

92 method in the ionospheric delay calculation procedure.

93 **2 SPP mathematical models**

94   In this section, the grounds of the common used SPP mathematical models using Klobuchar algorithm and IGS TEC

95 map will be introduced, and the proposition of the new strategy of SPP determination by use of simple as well as

96   autonomous method to estimate the ionospheric delay. This is followed by the appropriate algorithm presentations with

97   suitable explanations. In addition, the accuracy analysis criteria will be described in view of models credibility procedure.

2.1 SPP with ionospheric corrections using Klobuchar algorithm and IGS TEC map

99   In this study, the Klobuchar model was adapted as a reference in the SPP accuracy tests. Eight model coefficients

100 transmitted via navigation message are the primary components involved in the algorithm to reduce the ionosphere effect in

101 the SPP. The geodetic coordinates of the GPS antenna, GPS observing time (in seconds) as well as azimuth and elevation of

102 observed satellites as viewed from the receiver are needed to be known. The formula to calculate the ionospheric correction

103 based on the Klobuchar algorithm is as follows (Hofmann-Wellenhof et al., 2008):

104 $$\Delta T_V^{Iono} = A_1 + A_2 \cos\left(\frac{2\pi(t - A_3)}{A_4}\right) \tag{1}$$

105 where A_1 is a constant value of 5 ns. In turn, A_2 is a sum of multiplying four α coefficients and the geomagnetic latitude of

106 an ionospheric pierce point φ_{IP}^m. t means GPS time of the ionospheric pierce point. A_3 is 14:00 local time which specifies the

107 highest ionospheric disturbance. A_4 means the same as A_3 but there are four β coefficients are multiplied by φ_{IP}^m.

108 To obtain an ionospheric delay alongside the GPS signal travel path, the mapping function should be employed. Thus,

109 the concept of the ionospheric point has to be expanded as a piercing point of the GPS wave path and the

110 ionospheric single layer on the specified altitude. Thus, the zenith angle at the piercing point should first be indicated

111 (Hofmann-Wellenhof et al., 2008):

112 $$\sin z' = \frac{R_e}{R_e + h_m} \sin z_0 \tag{2}$$

113 R_e is Earth radius 6370 km and z_0 means a zenith angle from the receiver site. h_m is defined as the height of the ionospheric

114 pierce point. In general, h_m is identified by the single-layer model where all free electrons are concentrated in the infinitesimal

115 spherical shell at the assumed altitude - 450 km. Other formulations are possible too, for instance, from the Klobuchar

116 algorithm, presented in Rui et al. (2011):

117 $$mF = 1 + 16 \cdot \left(0.53 - \frac{E}{\pi}\right)^3 \tag{3}$$

118 where E means an elevation angle in the slant factor calculation.

119 It should be also noted that the type of mapping function in the atmospheric effect calculation process contributes to the

120 final solution accuracy as well. Allain et al. (2009) examined the tomographic mapping function known as Multi-Instrument

121 Data Analysis System (MIDAS) to ionospheric effect determination for the single-frequency data. Research has shown that

122 daily positioning errors are up to 50% lower in comparison to positioning using the Klobuchar algorithm or International

123   Reference Ionosphere (IRI) when the surrounding distribution of receivers is favorable. Regardless of the map type, dual-

124   frequency observations allow for even greater precision of the ionospheric effect mitigation in the GPS pseudo-range

125   measurement.

126   Therefore, the mapping function can be used as an inverse of the cosine function (Hofmann-Wellenhof et al., 2008):

127     $\Delta T_s^{Iono} = \Delta T_v^{Iono} / \cos z'$ (4)

128   Finally, the ionospheric delay alongside the rover-satellite is achieved in seconds. To obtain the metric magnitude of

129   the calculated effect, ΔT_s^{Iono} is multiplied by the speed of light. The Klobuchar algorithm was fully described by Xu (2007).

130   To future elaboration, ΔT_s^{Iono} will be denoted as δ_K where subscript is appropriate for the Klobuchar method.

131   The second approach is SPP with ionospheric corrections computed based on the IGS TEC map. This method is used to

132   examine and verify the quality of the new autonomous, estimation method of the ionospheric effect in the SPP.

133   Consequently, ionospheric delay as the base formula in the zenith direction can be introduced (Schüler, 2001):

134     $\delta_{IT} = \int\limits_{h_m}^{\infty} \frac{C_2}{f^2} = \frac{C}{f^2} \int\limits_{h_m}^{\infty} N_e(h) \cdot dh = \frac{C}{f^2} \cdot VTEC$ (5)

135   where the subscript is proper for the IGS TEC map product. C is a constant value of 40.3 m^3/s^2, f is an appropriate frequency,

136   and $VTEC$ is naturally the vertical total electron content in TECU units. N_e is electron density factor [electrons/m^3], and h is

137   equal to the travelled ray path from the satellite to the rover. In turn, h_m is the height of the single layer of the ionosphere or

138   height of the piercing point for which the appropriate VTEC value from IGS TEC is interpolating. Hence, there is a need to

139   indicate the geodetic coordinates for ionospheric pierce point using e.g. geometric method formulation (Prol et al., 2017).

140   Taking into account ionospheric delay as a proportional value to TEC and proportional to the distance covered across

141   the band, the relation of VTEC and TEC can be defined (Leick et al., 2015):

142     $VTEC = \cos z' \cdot TEC$ (6)

143   To integrate VTEC to STEC, the ionospheric mapping function, mentioned in the Eq. (2) is presented as an inverse of the

144   cosines function (Leick et al., 2015):

145     $F(z') = \frac{1}{\cos z'} = \left[1 - \left(\frac{R_e \sin z'}{R_e + h_m} \right)^2 \right]^{-\frac{1}{2}}$ (7)

146   where the adopted z' angle is equivalent to the zenith angle at the piercing point in (4).

147   Using Eq. (5), (6), and (7), the ionospheric correction can be obtained in the ray path direction between satellite-rover:

5

148 $$\delta_{IT} = \frac{40.3}{f^2} \cdot F(z') \cdot VTEC \qquad (8)$$

149   Therefore, to briefly explain the mathematical model of SPP with utilized ionospheric corrections, the code observation

150 equation was adapted based on Strang and Borre (2008) with complementary changes:

151 $$\begin{cases} P_r^s = \rho_r^s + c(\Delta t_r - \Delta t^s) + \delta_{TROP} + \delta_K + \varepsilon_P \\ P_r^s = \rho_r^s + c(\Delta t_r - \Delta t^s) + \delta_{TROP} + \delta_{IT} + \varepsilon_P \end{cases} \qquad (9)$$

152 where the first equation is concerning on the SPP approach with Klobuchar algorithm and the second one is referring

153 to the IGS TEC map. The left side is the measured pseudo-range. On the right side are the model and estimated magnitudes:

154 the geometrical distance between rover and satellite (satellite coordinates computed by utilization of the ephemeris

155 information – SP3 file), speed of light, receiver and satellite clock biases, tropospheric delay, ionospheric delay (computed

156 using Klobuchar algorithm (eight coefficients from navigation message) or IGS TEC map utilizing IONEX file) and pseudo-

157 range remaining error, respectively. In the research, the tropospheric corrections were obtained based on Hopfield (see

158 Hopfield, 1969) using model values of the dry and the wet subcomponents. Additionally, the clock bias of satellites has been

159 received by the utilization of satellites' ephemeris data and the relativistic improvements.

2.2 Modified SPP with autonomous VTEC estimation method

161   The essence of the proposed modified SPP method lies in an estimation of the $\Delta VTEC$ term which is a variable

162 component of the ionospheric delay:

163 $$\delta_{IONest} = \frac{40.3 \cdot 10^{16}}{f^2} \cdot F(z') \cdot (VTEC_0 + \Delta VTEC) \qquad (10)$$

164 the frequency in the real tests was adopted as the L1 carrier of the GPS signal: 1575.42 MHz.

165   The modified SPP model with an independent method of the ionospheric effect estimation is expressed in the system of

166 equations:

167 $$\begin{cases} P_1 = \rho_r^{s_1} + c(\Delta t_r - \Delta t^{s_1}) + \delta_{TROP_1} + \delta_{IONest_1} + \varepsilon_1 \\ P_2 = \rho_r^{s_2} + c(\Delta t_r - \Delta t^{s_2}) + \delta_{TROP_2} + \delta_{IONest_2} + \varepsilon_2 \\ \quad . \\ \quad . \\ \quad . \\ P_n = \rho_r^{s_n} + c(\Delta t_r - \Delta t^{s_n}) + \delta_{TROP_n} + \delta_{IONest_n} + \varepsilon_n \\ VTEC^{pseudoobs} = VTEC_0 + \Delta VTEC + \varepsilon_{\Delta VTEC} \end{cases} \qquad (11)$$

168   The last row is a pseudo-observation equation in which $VTEC_0$ is the constant, initial value of VTECs in a given epoch,

169   appropriate for all satellite elevation, $\Delta VTEC$ is an estimated ingredient and $\varepsilon_{\Delta VTEC}$ is a remaining error of determining factor. It

170   was decided, after performing many tests, to include this pseudo-observation equation into the SPP approach to ensure a

171   stable GPS solution. The model without the pseudo-observation formula would be too weak to give stable results (note that

172   single epoch positioning is used).

173   After many computational tests, it was assumed that the initial value of $VTEC_0$ in any measured epochs during daytime

174   and nighttime of SPP is **5 TECU.** Therefore, the method does not need external information about VTEC referring to the

175   piercing point on the line of sight receiver – satellite, even if the IGS TEC map is available, it indicates that the model is

176   simple to build and implement into a complex algorithm. The reliability and usefulness will be submitted during the

177   presentation of the results.

178   It is assumed in this method that the "observed" and approximate values are equal:

179
$$VTEC^{pseudoobs} = VTEC_0 \tag{12}$$

180   Continuing, to simplify successive descriptions of the modified SPP approach, the mapping coefficient is denoted:

181
$$mapcoeff = \frac{40.3 \cdot 10^{16}}{f^2} F(z') \tag{13}$$

182   The system of code equations (11) after linearization can be introduced in the matrix notation:

183
$$\mathbf{V} = \mathbf{AX} - \mathbf{L} \tag{14}$$

184   where:

185
$$\mathbf{V} = \begin{bmatrix} -\varepsilon_1 \\ \vdots \\ -\varepsilon_n \end{bmatrix} \tag{15}$$

186   is a residual vector,

187
$$\mathbf{A} = \begin{bmatrix} a_{11} & a_{12} & a_{13} & 1 & \vdots\ mapcoeff^1 \\ \vdots & \vdots & \vdots & \vdots & \vdots \\ a_{n1} & a_{n2} & a_{n3} & 1 & mapcoeff^n \\ 0 & 0 & 0 & 0 & 1 \end{bmatrix} \tag{16}$$

188   is a design matrix.

189   The vector of unknowns receives an additional parameter in the adjustment process:

190 $\mathbf{X} = \begin{bmatrix} \Delta X_r \\ \Delta Y_r \\ \Delta Z_r \\ c\Delta t_r \\ \hdashline \Delta VTEC \end{bmatrix}$ (17)

191   The disclosure vector is:

192 $\mathbf{L} = \begin{bmatrix} L_r^1 \\ \vdots \\ L_r^n \\ \hdashline 0 \end{bmatrix}$ (18)

193   where $L_r^i = P_i - \rho_i^r + c\Delta t^i - \delta_{TROP_i} - mapcoeff \cdot VTEC_0$. The last entry amounts to zero because of assumption (12).

194   The weight matrix has been prepared based on pseudo-range measurement error which was assumed as a 2.00 m and

195   appropriate satellite elevation angle. The criterion of the minimal mask was implemented as a 10 degree. After

196   computational tests with theoretical analysis, the weight of the estimated component $\Delta VTEC$ was assumed in the model as 1.

197 $\mathbf{P} = \begin{bmatrix} \frac{1}{\delta^2}\sin(elev_1) & \dots & 0 & 0 \\ \vdots & \ddots & \vdots & \vdots \\ 0 & \dots & \frac{1}{\delta^2}\sin(elev_n) & 0 \\ \hdashline 0 & \dots & 0 & 1 \end{bmatrix}$ (19)

198   The least-squares estimate of the Eq. (14) is computed from the normal equations:

199 $\mathbf{A^TPA\hat{X} - A^TPL = 0}$ (20)

200   together with its covariance matrix:

201 $\mathbf{C_{\hat{x}} = m_0^2 (A^TPA)^{-1}}$ (21)

202   with the variance factor: $m_0^2 = \frac{\mathbf{V^TPV}}{n-m}$.

203   The number of parameters $m = 5$. Thus, the minimal number of observations should be $n = 6$ to ensure necessary

204   redundancy.

205   **2.3 Accuracy analysis criteria**

206   The basic statistical operator in the experiment is a distance of the solution from the true position (*dist*) as well as its

207   average value (*DIST*), computed from solutions obtained from the single epochs with its mean error. The actual position

Geoscientific
Instrumentation
Methods and
Data Systems

Discussions

Open Access

208 means constant station coordinates provided by the agency, which manage the Continuously Operating Reference Station

209 (CORS) used in the experiment for evaluation of the positioning model accuracy. The formula can be introduced in each

210 epoch as follows:

211 $$dist_{ep_i} = \sqrt{(X_r - X_t)^2 + (Y_r - Y_t)^2 + (Z_r - Z_t)^2}$$ (22)

212 where subscript "r" means calculated rover's coordinates and "t" regarding to the actual position.

213   Therefore:

214 $$m^2_{dist_{ep_i}} = \mathbf{W} \mathbf{C}_{\hat{X}_{ep_i}} \mathbf{W'}$$ (23)

215 where $\mathbf{C}_{\hat{X}}$ is a covariance matrix of the parameter vector and $\mathbf{W}$ is a gradient:

216 $$\mathbf{W} = \left[\frac{\Delta X_{ep_i}}{dist_{ep_i}} \quad \frac{\Delta Y_{ep_i}}{dist_{ep_i}} \quad \frac{\Delta Z_{ep_i}}{dist_{ep_i}} \right]$$ (24)

217   The average value is as follows:

218 $$m^2_{DIST} = \frac{1}{n^2} \sum_{i=1}^{n} m^2_{dist_{ep_i}}$$ (25)

219   The NEU (North East Up) coordinates system was used in the comparative analysis, where the calculated rover's

220 position is compared to the actual position. Therefore, the rotation matrix was used to convert the covariance matrix (21) of

221 the parameters to the NEU system:

222 $$\mathbf{C}_{\mathbf{NEU}} = \mathbf{R} \mathbf{C}_{\hat{X}} \mathbf{R}^T$$ (26)

223 where:

224 $$\mathbf{R} = \begin{bmatrix} -\sin\varphi\cos\lambda & -\sin\varphi\sin\lambda & \cos\varphi \\ -\sin\lambda & \cos\lambda & 0 \\ \cos\varphi\cos\lambda & \cos\varphi\sin\lambda & \sin\varphi \end{bmatrix}$$ (27)

225 The φ and λ are rover geodetic coordinates.

226   The covariance matrix of mean values computed from the whole observational day is:

227 $$\mathbf{C}_{\mathbf{NEU}_{mean}} = \mathbf{D} \mathbf{C}_{\mathbf{NEU}_{set}} \mathbf{D}^{\mathbf{T}} = \frac{1}{n^2} \sum_{i=1}^{n} \mathbf{C}_{\mathbf{NEU}_{ep_i}}$$ (28)

228 where $\mathbf{C}_{\mathbf{NEU}_{set}}$ is a block matrix which contains on the diagonal the covariance matrixes in the NEU setup from all measured

229 epochs (n) and $\mathbf{D}$ is treated as a transition matrix from the NEU to their mean values:

230 $$\mathbf{D} = \begin{bmatrix} \frac{1}{n} & 0 & 0 & \frac{1}{n} & 0 & 0 & \cdots & \frac{1}{n} & 0 & 0 \\ 0 & \frac{1}{n} & 0 & 0 & \frac{1}{n} & 0 & \cdots & 0 & \frac{1}{n} & 0 \\ 0 & 0 & \frac{1}{n} & 0 & 0 & \frac{1}{n} & \cdots & 0 & 0 & \frac{1}{n} \end{bmatrix}$$ (29)

3 Numerical experiment and discussion

232 In this section, the explanation of the research concept will be done. Next, the appropriate numerical experiment in
233 view of graphics and numeric settings. The parallel discussion about obtained results for appropriate interpretation will be
234 made.

3.1 Research concept

236 The numerical experiment is based on real single frequency code pseudorange observations. Namely, C1C code data on
237 the L1 carrier frequency (1575.42 MHz). Continuing, three different EURE Permanent GNSS Network stations have been
238 chosen in Scandinavia. Two stations in Sweden – Visby (VIS) and Skellefteå (SKE), one in Norway – Vardø (VARS). The
239 observational files and initial coordinates of receivers was gained from the BKG (Bundesamt für Kartographie und
240 Geodäsie) GNSS Data Center. The parameters of satellite orbits (SP3 file) and atmospheric data were obtained by means of
241 CDDIS (Crustal Dynamics Data Information System) - in fact, IONEX (IONosphere map EXchange format) only in view of
242 atmospheric data, as a source of IGS TEC map. The coordinates of points were treated as the true coordinates in the practical
243 part of the experiment. The reference coordinates are presented in the table:

244 **Table 1.** Actual coordinates of points

Points	X	Y	Z
VIS600SWE	3246466.556	1077901.829	5365279.606
SKE800SWE	2534032.877	9751679.370	5752078.718
VARS00NOR	1844607.623	1109719.107	5983936.007

245

246 In the models, the actual coordinates have been converted to the antenna phase center to make a comparative analysis with
247 the SPP results, where measurements were executed to the antenna phase center.

248 Three different localizations allow checking how the modified SPP model works on different geodetic latitude because
249 of ionosphere activity changes, so its quality in the GPS code domain can be widely stated.

250 The research concept focuses on measurement on two different days in the cited locations. Therefore, three stations of
251 the EUREF Permanent GNSS Network were employed for comparative analysis based on data from two parallel days. The
252 table below presents the structure of the experiment:

10

Table 2. Experiment concept

Points	Days	SPP methods
VIS600SWE	15/06/2019 15/08/2019	SPPwithKM (SPP with Klobuchar model) MSPPwithdVTEC (Modified SPP with **Δ**VTEC estimation) SPPwithITM (SPP with IGS TEC map)
SKE800SWE	15/06/2019 15/08/2019	SPPwithKM MSPPwithdVTEC SPPwithITM
VARS00NOR	15/06/2019 15/08/2019	SPPwithKM MSPPwithdVTEC SPPwithITM

To execute the practical part of the research, the MATLAB environment from The MathWorks was used. The "PostCalc" software developed by Dawid Kwaśniak was implemented with the complementary changes done by the authors.

3.2 Discussion of the experiment results

The Figures 1-3 present the distribution of *dist* values during the observational day (*Results of the positioning models*) and their average value *DIST* with appropriate mean errors in the middle (*Average results of the positioning models*). In turn, the bottom parts show the error reduction of the models (*Differences of the positioning models*). The upper part of Figure 1(**a**) demonstrates the solutions for Visby station on 15 June, 2019. The *dist* results are significantly improved for **MSPPwithdVTEC** referring to the **SPPwithKM** what is confirmed by the average value of *DIST* equalled to 4.886 m. There is not a major difference of *DIST* between **MSPPwithdVTEC** and **SPPwithITM** (0.033 m). Therefore, the mean error of *DIST* (0.072 m) affirms the precision of the modified solution. Studying the bottom division of Figure 1(**a**), **SPPwithKM** was assumed as a reference one (100%) in the calculation of the percent values of error reduction based on *DIST*. The results are satisfying because of error reduction on the level of 22.97% in the **MSPPwithdVTEC** case and the close discrepancy with the error reduction of the **SPPwithITM** (0.53%). The second day using Visby station is 15 August, 2019. In the middle of Figure 1(**b**), *DIST* is beneficial for the **MSPPwithdVTEC** (4.912 m) compared to the reference model which leads to defining the tendency of improved accuracy in the SPP. Again, the difference in the average solutions of *DIST* between **MSPPwithdVTEC** and **SPPwithITM** is insignificant (0.055 m) according to code observations accuracy level. Thus, the accuracy of the estimation method is comparable with the IGS TEC map. Focusing on the average explanation of the *DIST* mean errors among the **MSPPwithdVTEC** (0.067 m) and the **SPPwithITM** (0.074 m), these approaches do not distinctly vary, which indicates that the proposed SPP model works well. In the bottom of Figure 1(**b**), the error reduction of **MSPPwithdVTEC** is 20.90% and is at a similar level with **SPPwithITM** (21.79%). The **SPPwithKM** proved to be the lowest accuracy method. Probably, the ionospheric corrections obtained by the coefficients from the navigation message cannot reflect the changes that take place in the ionosphere with the higher temporal accuracy. Briefly, in the first studied point, the **MSPPwithdVTEC** can be judged as the precise SPP model.

Geoscientific
Instrumentation
Methods and
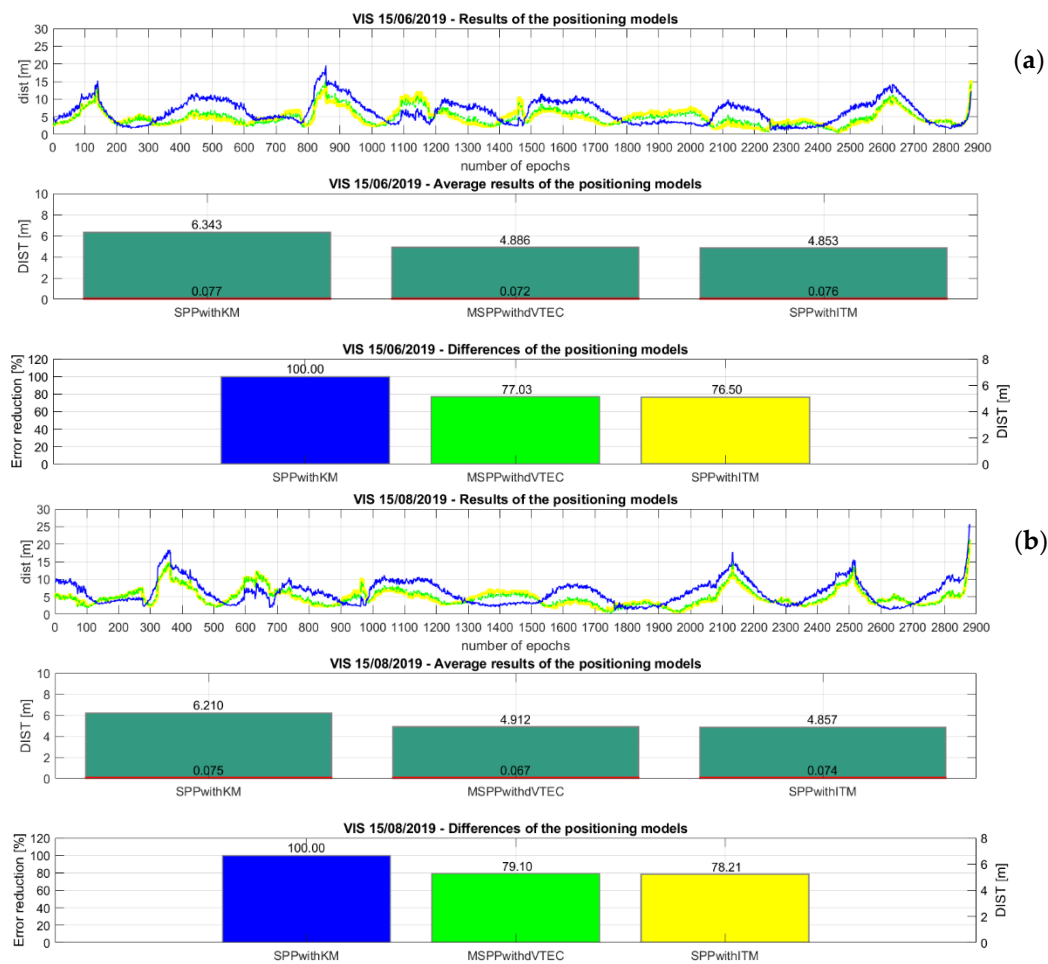Data Systems
Discussions

Open Access

Figure 1. Set of the results of the positioning models: (**a**) VIS 15/06/2019 (**b**) VIS 15/08/2019

Following the experiment report, the next examined subject is SKE 15/06/2019. Looking at Figure 2(**a**), the top part presents the *dist* distribution of the **MSPPwithdVTEC** solutions close to the **SPPwithITM**. The average description of *DIST* validates this declaration, where the difference between these two approaches is 0.017 m, in favor of the **MSPPwithdVTEC**. In turn, according to the base model, the **MSPPwithdVTEC** delivers solutions with highly-increased accuracy, which is the most important. Despite such accuracy, the *DIST* precision of **MSPPwithdVTEC** (0.080 m) is improved and is at a similar level as **SPPwithITM** (0.093 m), which confirms the consistency of the methods. Explaining the bottom part of Figure 2(**a**), the error reduction of the **MSPPwithdVTEC** is at the beneficial level of 22.55%, which is again close to the reduction obtained by **SPPwithITM** (22.30%). Therefore, this method can be evaluated as the approach of a similar class compared to the case with IGS TEC map. The second day of tests is 15 August 2019. Based on *dist* in the top of Figure 2(**b**), it is noticeable that the **MSPPwithdVTEC** results are at related relatively similar level as **SPPwithITM.** Looking in the middle part of Figure 2(**b**), the increased accuracy in **MSPPwithdVTEC** is verified by the *DIST* solution

311   equal to 5.354 m, referring to the initial **SPPwithKM**. The mean error of *DIST* gives an acceptable value using

312   **MSPPwithdVTEC** by comparable magnitude with the other models. Considering the bottom part of Figure 2(**b**), the error

313   reduction amounts to 21.30% whereas the approach with the IGS TEC map achieves an equivalent value of 21.07%. In sum,

314   the **MSPPwithdVTEC** can be assessed on the next EUREF's location as the valuable SPP approach by use of the new

315   method of the ionospheric refraction estimation, without the need for external products, e.g. atmospheric factors or GIMs.
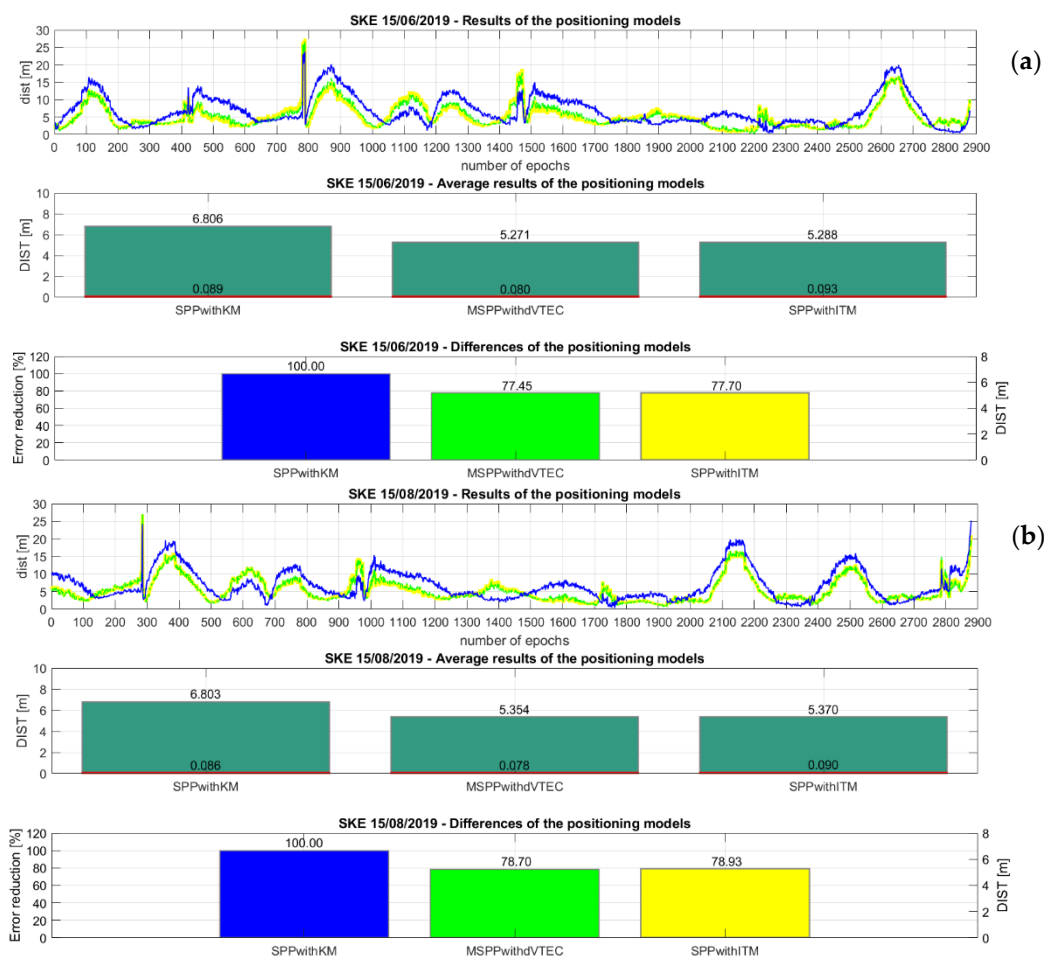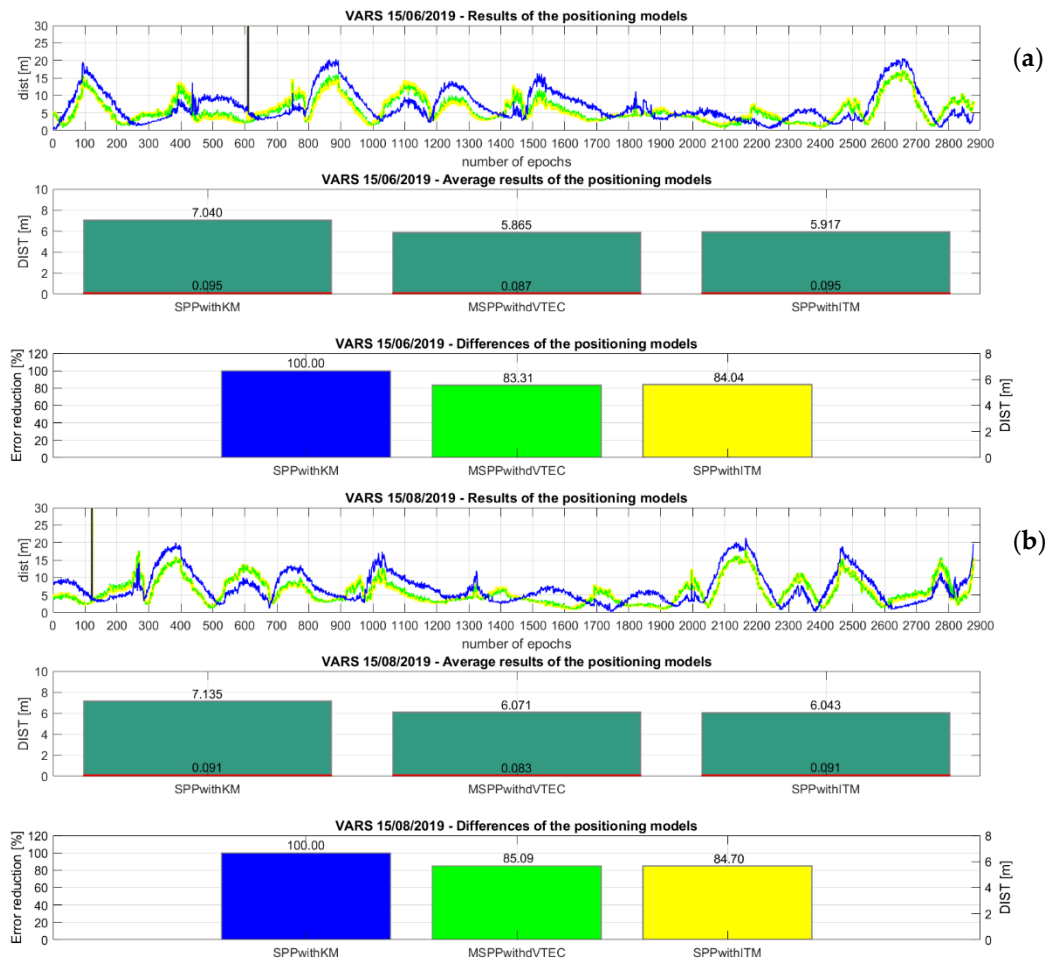

Figure 2. Set of the results of the positioning models: (**a**) SKE 15/06/2019 (**b**) SKE 15/08/2019

334   The last studied point is VARS00NOR. The first examined day is 15 June 2019. The middle part of Figure 3(**a**)

335   demonstrates that the *DIST* difference of the two approaches: **SPPwithITM** and **MSPPwithdVTEC** is 0.052 m, therefore

336   the improved accuracy is at a similar level, referring to **SPPwithKM** average observations. The precision of *DIST* confirms

337   the reliability of the **MSPPwithdVTEC**, where the mean error is equal to 0.087 m with an insignificant discrepancy

338   (0.008 m) compared to the **SPPwithITM**. The bottom part of Figure 3(**a**) shows a decrease in the percent value of the error.

339   The error reduction of the **MSPPwithdVTEC** is at the level of 16.69%, thus the improvement of accuracy is verified. Again,

340   the difference of error reduction among **MSPPwithdVTEC** and **SPPwithITM** is on the parallel level (0.73%) which
341   confirms the method credibility. The second tested day, and therefore the last one, is 15 August 2019. The *DIST* elaboration
342   in Figure 3(**b**) presents the low differences between the two principal approaches on the level of 0.028 m. Studying the
343   bottom division of Figure 3(**b**), the **MSPPwithdVTEC** achieves a positive level of error reduction of 14.91%, relating to the
344   **SPPwithKM**. In addition, the top parts of Figure 3 (**a**) and (**b**) present the distribution of **MSPPwithdVTEC** *dist* results as
345   close in value to the **SPPwithITM** with increased accuracy to **SPPwithKM**. This finding is also valid to other examined
346   cases. Thus, the proposed model can be identified as stable and accurate. The error reduction is at a satisfactory level.

Figure 3. Set of the results of the positioning models: (**a**) VARS 15/06/2019 (**b**) VARS 15/08/2019

365   Focusing on the mean errors of the final solution in the NEU system, we will consider the average precision of the
366   differences of the components ΔN, ΔE, and ΔU, referring to the daily result. The difference means the discrepancy between
367   the actual station's coordinates and the received position from the SPP methods. For this purpose, the Eq. (28) was used to
368   determine the mean values of ΔN, ΔE and ΔU errors which are summarized in the table below:

369   **Table 3.** Average errors of the difference in the positions using the NEU system

SPP method	$m_{\Delta N}$	$m_{\Delta E}$	$m_{\Delta U}$	Station and Day
SPPwithKM	0.06	0.04	0.10	
MSPPwithdVTEC	**0.05**	**0.04**	**0.09**	VIS 15/06/2019
SPPwithITM	0.06	0.04	0.09	
SPPwithKM	0.06	0.04	0.09	
MSPPwithdVTEC	**0.06**	**0.03**	**0.08**	VIS 15/08/2019
SPPwithITM	0.06	0.04	0.09	
SPPwithKM	0.05	0.03	0.11	
MSPPwithdVTEC	**0.04**	**0.03**	**0.10**	SKE 15/06/2019
SPPwithITM	0.05	0.03	0.11	
SPPwithKM	0.05	0.03	0.11	
MSPPwithdVTEC	**0.04**	**0.03**	**0.10**	SKE 15/08/2019
SPPwithITM	0.05	0.03	0.11	
SPPwithKM	0.04	0.03	0.11	
MSPPwithdVTEC	**0.04**	**0.03**	**0.10**	VARS 15/06/2019
SPPwithITM	0.04	0.03	0.11	
SPPwithKM	0.04	0.03	0.11	
MSPPwithdVTEC	**0.04**	**0.03**	**0.10**	VARS 15/08/2019
SPPwithITM	0.04	0.03	0.11	

370
371   The error quantities of the difference in the positions were achieved for **MSPPwithdVTEC** and **SPPwithITM** on a

372   close level**.** Separating the horizontal and the vertical components of the position, the **MSPPwithdVTEC** is characterized by

373   improved precision compared to **SPPwithKM** in the North and East direction, therefore, the additional estimated parameter

374   in the code equation does not change the SPP model enough to reduce its quality. The case is repeated in the context of the

375   vertical component U, the **MSPPwithdVTEC** is again profitable to **SPPwithKM** and achieves the similar values of the

376   mean errors to **SPPwithITM**. In general, the values of mean errors are close to each other and the differences are not as clear

377   in the context of the code data use. Therefore, the quantities of average errors demonstrate that **MSPPwithdVTEC** is the

378   approach of the closest precision to the SPP method with an IGS TEC map, specified as a high-quality product, which is the

379   most important from the authors' point of view.

380   **4 Conclusions and future perspectives**

381   The main idea of this paper was to introduce the new method to estimate the ionospheric delay in the SPP without using

382   the external data. Moreover, in the case of comparative analysis, two common approaches in SPP was employed: SPP with

383   Klobuchar algorithm and SPP with IGS TEC map. The first one was treated as a reference one. The SPP model with IGS

384   TEC map was utilized to authenticate the proposed model in view of IGS TEC map use - defined as a high-quality product.

385   The explanation of mathematical models and appropriate accuracy analysis criteria was done. Next, the numerical

386   experiment using real code data from three different GNSS stations with discussion to interpret the obtained results.

Geoscientific
Instrumentation
Methods and
Data Systems
Discussions

387 Referring to achieved solutions, the proposed approach can be defined as a simple and independent way to improve SPP.

388 Moreover, the **MSPPwithdVTEC** can be employed in the procedure of determination the approximate position for the need

389 of the single-epoch precise positioning.

390 Based on the mean distance of the solution from the true position, the **MSPPwithdVTEC** achieved improved GPS

391 position in comparison to the basic **SPPwithKM** in each tested station. Moreover, the **MSPPwithdVTEC** acquires a similar

392 level of error reduction to the **SPPwithITM** what is the most satisfying in view of method authentication.

393 Finally, the results of the **MSPPwithdVTEC** confirm the potential use of the mathematical model in the SPP. The

394 strategy should be developed in the future through the verification of model stability in the other stations since ionosphere

395 changes are highly dependent on localization. Therefore, the proposed method of SPP can be recognized as a good forecast

396 to become independent of external products delivering information about the ionospheric delay.

399 **References**

400 Abdelazeem, M., Çelik, R., and El-Rabbany, A.: An Enhanced Real-Time Regional Ionospheric Model Using IGS Real-
401 Time Service (IGS-RTS) Products, The Journal of Navigation, 69, 521-530, https://doi.org/10.1017/S0373463315000740,
402 2016.

403 Allain, D.J. and Mitchell, C.N.: Ionospheric delay corrections for single-frequency GPS receivers over Europe using
404 tomographic mapping, GPS Solutions, 13, 141-151, https://doi.org/10.1007/s10291-008-0107-y, 2009.

405 Awange, J.L.: Environmental Monitoring using GNSS, 1st ed., Springer-Verlag, Berlin/Heidelberg, Germany, 2012.

406 Bakuła, M.: Precise Method of Ambiguity Initialization for Short Baselines with L1-L5 or E5-E5a GPS/GALILEO Data,
407 Sensors, 18, 4318, https://doi.org/10.3390/s20154318, 2020.

408 Bosy, J.: Scientific journals of the Agricultural Academy in Wrocław CCXXXIV (no. 522): Precise Processing of satellite
409 GPS observations in local networks located in mountain areas, 1st ed., Publishing house of the Agricultural Academy,
410 Wrocław, Poland, 2005.

411 Chen, K. and Gao, Y.: Real-Time Precise Point Positioning Using Single-Frequency Data, in: Proceedings of the 18th
412 International Technical Meeting of the Satellite Division of The Institute of Navigation, Long Beach, USA, September 2005.

413 Ciećko, A. and Grunwald, G.: Klobuchar, NeQuick G, and EGNOS Ionospheric Models for GPS/EGNOS Single-
414 Frequency Positioning under 6-12 September 2017 Space Weather Events, Applied Sciences, 10, 1553,
415 https://doi.org/10.3390/app10051553, 2020.

416 Ciraolo, L.: Ionospheric Total Electron Content (TEC) from the Global Positioning System, in: Proceedings of the XXVIIIth
417 URSI General Assembly, New Delhi, India, October 2005.

418 Cooper, C., Mitchell, C.N., Wright, C.J., Jackson, D.R., and Witvliet, B.A.: Measurement of Ionospheric Total
419 Electron Content Using Single-Frequency Geostationary Satellite Observations, Radio Science, 54, 10-19,
420 https://doi.org/10.1029/2018RS006575, 2019.

421 de Camargo, P.O., Monico, J.F.G., and Ferreira, L.D.D.: Application of ionospheric corrections in the equatorial region for
422 L1 GPS users, Earth Planet Space, 52, 1083-1089, https://doi.org/10.1186/BF03352335, 2000.

423 El-Rabbany, A.: Introduction to GPS: The Global Positioning System, 1st ed., Artech House Mobile Communications Series,
424 Norwood, USA, 2002.

425 Georgiadiou, P.Y.: Modeling the ionosphere for an active control network of GPS stations, LGR - series: publications of the
426 Delft Geodetic Computing Centre, 7, 1994.

427 Golubkov, G.V., Manzhelii, M.I. and Eppelbaum, L.V.: Quantum Theory of Disturbance and Delay of GPS Signals in D and
428 E Atmospheric Layers: An Introduction, Positioning, 9, 13-22, https://doi.org/10.4236/pos.2018.92002, 2018.

429 Golubkov, G.V., Manzhelii, M.I. and Eppelbaum, L.V.: Quantum Nature of Distortion and Delay of Satellite Signals II,
430 Positioning, 9, 47-72, https://doi.org/10.4236/pos.2018.93004, 2018.

431 Hofmann-Wellenhof, B., Lichtenegger, H., and Wasle, E.: GNSS – Global Navigation Satellite Systems, 1st ed., Springer-
432 Verlag, Wien, Austria, 2008.

433 Hopfield, H.S.: Two-quartic tropospheric refractivity profile for correcting satellite data, Oceans and Atmospheres, 74, 4487-
434 4499, https://doi.org/10.1029/JC074i018p04487, 1969.

435 Klobuchar, J.A.: Ionospheric Time-Delay Algorithm for Single-Frequency GPS Users, IEEE Transactions on Aerospace and
436 Electronic Systems, AES-23, 325-331, https://doi.org/10.1109/TAES.1987.310829, 1987.

437 Krypiak-Gregorczyk, A., Wielgosz, P., and Borkowski, A.: Ionosphere Model for European Region Based on Multi-GNSS
438 Data and TPS Interpolation, Remote Sensing, 9, 1221, https://doi.org/10.3390/rs9121221, 2017.

439 Krypiak-Gregorczyk, A. and Wielgosz, P.: Carrier phase bias estimation of geometry-free linear combination of GNSS
440 signals for ionospheric TEC modeling, GPS Solutions, 22, 45 (2018), https://doi.org/10.1007/s10291-018-0711-4, 2018.

441 Kuverova, V.V., Adamson, S.O., Berlin, A.A., Bychkov, V.L., Dmitriev, A.V., Dyakov, Y.A., Eppelbaum, L.V., Golubkov,
442 G.V., Lushnikov, A.A., Manzhelii, M.I., Morozov, A.N., Nabiev, S.S., Suvorova, A.V., Golubkov, M.G.: Chemical physics
443 of D and E layers of the ionosphere, Ad. in Space Research, 63, 1876-1886, https://doi.org/10.1016/j.asr.2019.05.041, 2019.

444 Leick, A., Rapoport, L., and Tatarnikov, D.: GPS Satellite Surveying, 4th ed., John Wiley & Sons, Hoboken, USA, 2015.

445 Prol, F.S., Camargo, P.O., and Muella, M.T.A.H.: Comparative study of methods for calculating ionospheric points and
446 describing the GNSS signal path, Boletim de Ciências Geodésicas, 23, 669-683, http://dx.doi.org/10.1590/s1982-
447 21702017000400044, 2017.

448 Rui, T., Qin, Z., Guanwen, H., and Hong, Z.: On ionosphere-delay processing methods for single-frequency precise-point
449 positioning, Geodesy and Geodynamics, 2, 71-76, https://doi.org/10.3724/SP.J.1246.2011.00071, 2011.

450 Setti Júnior, P.T., Alves, D.B.M., and Silva, C.M.: Klobuchar and Nequick G ionospheric models comparison for multi-
451 GNSS single-frequency code point positioning in the Brazilian region, Boletim de Ciências Geodésicas, 25, e2019016,
452 https://doi.org/10.1590/s1982-21702019000300016, 2019.

453 Stępniak, K.: Analysis on the influence of advanced GNSS signal tropospheric delay modeling methods on estimated
454 coordinates of ASG-EUPOS stations, Ph. D. thesis, University of Warmia and Mazury, Olsztyn, 2016.

455 Strang, G. and Borre, K.: Linear Algebra, Geodesy, and GPS, 1st ed., Wellesley-Cambridge Press, Wellesley, USA, 2008.

456 Schüler, T.: On Ground-Based GPS Tropospheric Delay Estimation, Ph.D. thesis, Bundeswehr University, München, 2001.

457 Teunissen, P.J.G. and Kleusberg, A.: GPS for Geodesy, 2nd ed., Springer-Verlag, Berlin/Heidelberg, Germany, 1998.

458 US Army Corps of Engineers: NAVSTAR Global Positioning System Surveying, 2nd ed., Department of the Army US Army
459 Corps of Engineers, Washington, USA, 2003.

460 Xu, G.: GPS Theory, Algorithms and Applications, 2nd ed., Springer-Verlag, Berlin/Heidelberg, Germany, 2007.

461 Xu, G. and Xu, Y.: GPS Theory, Algorithms and Applications, 3rd ed., Springer-Verlag, Berlin/Heidelberg, Germany, 2016.

462 Zhang, L., Yao, Y., Peng, W., Shan, L., He, Y., and Kong, J.: Real-Time Global Ionospheric Map and Its Application in
463 Single-Frequency Positioning, Sensors, 19, 1138, https://doi.org/10.3390/s19051138, 2019.